Nanoscale

Accepted Manuscript

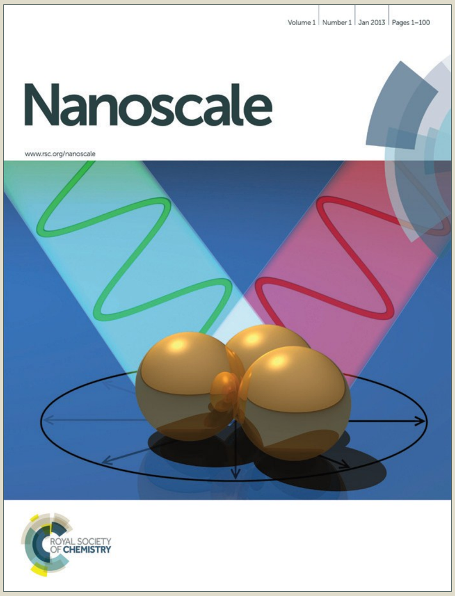

ROYAL SOCIETY OF CHEMISTRY

www.rsc.org/nanoscale

Journal Name

ARTICLE

Designing Molecular Structure to Achieve Ductile Fracture Behavior in a Stiff and Strong 2D Polymer, "Graphylene"

Received 00th January 20xx,
Accepted 00th January 20xx

DOI: 10.1039/x0xx00000x

www.rsc.org/

E. Sandoz-Rosado,[a] T.D. Beaudet,[a] R. Balu[b] and E.D. Wetzel[a]

As the simplest two-dimensional (2D) polymer, graphene has immensely high intrinsic strength and elastic stiffness but has limited toughness due to brittle fracture. We use atomistic simulations to explore a new class of graphene/polyethylene hybrid 2D polymer, "graphylene," that exhibits ductile fracture mechanisms and has a higher fracture toughness and flaw tolerance than graphene. A specific configuration of this 2D polymer hybrid, denoted "GrE-2" for the two-carbon-long ethylene chains connecting benzene rings in the inherent framework, is prioritized for study. MD simulations of crack propagation show that the energy release rate to propagate a crack in GrE-2 is twice that of graphene. We also demonstrate that GrE-2 exhibits delocalized failure and other energy-dissipating fracture mechanisms such as crack branching and bridging. These results demonstrate that 2D polymers can be uniquely tailored to achieve a balance of fracture toughness with mechanical stiffness and strength.

Introduction

While the study of 2D materials has been ongoing for the past decade, the study of 2D polymers is a recently emerging field[1, 2] due to several inherent advantages over typical 2D materials. Firstly, 2D materials such as graphene, transition metal dichalcogenides, and hexagonal boron nitride, are produced using techniques that are difficult for bulk scaling such as exfoliation or chemical vapor deposition (CVD). In contrast, bulk solution synthesis of 2D polymers has been demonstrated[1, 3-6]. Additionally, and perhaps more importantly, 2D polymers offer the ability to tailor material properties through organic molecular design. While the focus of the community has largely been on the synthesis and structure of emergent 2D polymers, less consideration has been given to their mechanical properties. Linear polymers like Nylon, Kevlar and polyethylene are already some of the strongest, stiffest and toughest materials per weight, illustrating the great potential that exists for optimizing a novel 2D polymer for structural and ballistic applications. Furthermore, the ability to tailor pore size and chemistry within a mechanically robust 2D covalent bond network should enable high performance selective membranes for applications such as water desalination and purification, chemical and biological filtration, and pharmacological processing.

As a benchmark material, graphene can be considered the simplest 2D polymer, consisting exclusively of sp^2-bonded C. The extraordinary in-plane stiffness and intrinsic strength of graphene[7] have made it a desirable candidate as a structural material. CVD of large-area graphene has advanced[8] to a level of maturity such that grain boundaries in CVD graphene approach the breaking strength of perfect crystalline graphene[9], a phenomenon that has also been predicted by atomistic simulations[10]. Graphene has the theoretical potential to enable ballistic barriers that have 10-100× less weight than barriers composed of Kevlar with the same ballistic limit[11], and has also demonstrated a specific kinetic energy of penetration an order of magnitude greater than steel and 2-3x greater than Kevlar, as measured by microscale ballistic experiments[12]. However, because graphene is a network of very stiff sp^2 bonds, it is highly resistant to fracture initiation. However, once formed, a crack will propagate in a brittle manner[13, 14]. This brittle behavior may limit graphene's potential as a structural engineering material, as local failure due to a flaw or stress concentration is likely to trigger a sudden and catastrophic global failure.

To demonstrate a 2D material with a more ductile fracture response compared to graphene, we propose a new family of 2D polymer which we refer to as "graphylene." This 2D covalent polymer network can be conceptually described as a graphene/polyethylene hybrid comprising benzene (C_6) rings linked by short polyethylene chains. These short polyethylene links give graphylene in-plane stiffness and strength values that are somewhat lower than graphene. However, we demonstrate that the flexibility of the sp^3 bonded carbon atoms in the polyethylene chains leads to ductile fracture propagation behavior, with significantly higher energy required to propagate cracks relative to graphene.

Graphene-like 2D polymers with sp^3 functionalization have been recently described. Graphane[15] adds single hydrogen bonds to each carbon atom in graphene, resulting in a hexagonal network of sp^3 bonds. Since the lattice structure remains simple hexagonal, it is unlikely to possess all of the toughening mechanisms available in the more extended graphylene network. Studies have also examined carbon allotropes that are randomly hydrogen functionalized, with failure surfaces exhibiting features indicative of toughening[16]. Graphyne[17] is composed of benzene C_6 rings bridged by sp^1-functionalized bridge units. These bridge units have been shown to promote crack arrest and more tortuous crack propagation[18, 19], but will be less compliant and flexible than the sp^3 bridge units in graphylene, and existing studies have not quantified

---

[a] 4600 Deer Creek Loop, Army Research Lab, Aberdeen Proving Ground, MD
[b] 2800 Powder Mill Road, Army Research Lab, Adelphi, MD.

Electronic Supplementary Information (ESI) available. See DOI: 10.1039/x0xx00000x

fracture properties. The polyethylene links in the graphylene 2D polymer structure should add compliance mechanisms that are not present in graphene, graphyne, graphane, or other 2D carbon allotropes, allowing for local ductility and greater flaw tolerance.

Establishing the Structure of Graphylene

We have broadly considered the graphylene-*n* (GrE-*n*) family of 2D polymers, where *n* indicates the characteristic length of the polyethylene (PE) chains in terms of the number of methylene bridge units ($-CH_2-$) between each nearest neighbor C_6 ring. A complete description of the various GrE-*n* configurations considered is provided in the Supplemental Information, with the results summarized as follows. Since the system is composed of rigid graphene units (C_6 rings) and more compliant polyethylene $(CH_2)_n$ units, we hypothesize that global stiffness and strength will reduce, while fracture toughness will increase, with increasing *n*. Simulations of various GrE-*n* polymers revealed that odd *n* configurations were more difficult to solve for converged stable states compared to even *n* configurations, primarily due to symmetry challenges that required larger unit cells and computational domain sizes. Therefore, although odd *n* graphylene systems are likely to be physically realizable, only even *n* systems were considered for further study. Of the possible *n* = 2, 4, 6, etc. configurations, GrE-2 polymers were selected as our system of interest as the closest comparison to graphene.

The GrE-2 system itself possesses multiple stable configurations. To identify the most stable and likely of these configurations, enthalpy calculations were performed to identify the lowest energy, highest density structure. These calculations were done via first-principles quantum mechanics density functional theory (DFT), by computing the ground state (2D) enthalpy curves under negative planar stress. **Figure 1** compares two of these configurations: "System A", in which the carbon atoms are nearly co-planar with the methylene bond angles accommodated in the plane; and "System B", in which the methylene bond angles are accommodated by allowing the carbon atoms in the polyethylene (PE) bridge units to position out-of-plane relative to the C_6 rings. The calculations show that System B is both lower energy and higher density than System A, and is therefore used for all subsequent GrE-2 calculations in this study. An interesting feature of System B is that it possesses rectangular symmetry: close inspection of the structure shows that, as one travels around a C_6 ring, the bridge bond angles are arranged UUUDDD, where "U" is up (carbon atoms above the central plane, Fig. 1b) and "D" is down (carbon atoms are below the central plane, Fig.1b) . This structure was found to be more energetically favorable than, for example, a UDUDUD structure. The rectangular symmetry of System B is necessary to allow the C_6 ring to tilt slightly out-of-plane, resulting in a more compact structure than if the rings were forced to reside fully in-plane.

Elastic Modulii of Graphylene. First-principles DFT uniaxial stress calculations for both the 1st and 2nd C_6 nearest-neighbor (1NN and 2NN, respectively) directions of GrE-2 were performed to determine its strength and stiffness, and to benchmark subsequent molecular dynamics (MD) predictions.

The elastic modulii were extracted from this stress-strain response during uniaxial tensile testing according to the following relationship:

$$\sigma_{2D} = E_{2D}\epsilon + D_{2D}\epsilon^2 \qquad (1)$$

where σ_{2D} is the 1st Piola-Kirchhoff stress, ϵ is engineering strain, and E_{2D} and D_{2D} are the first and second order elastic modulii respectively[11]. Because graphylene is being studied as an atomically-thin sheet, the stress and moduli values are expressed in units of [N/m]. In-plane elastic modulii are calculated by curve fitting the DFT data with Eq.1 to find E_{2D} and D_{2D} for the 1NN and 2NN lattice directions.

Analogous uniaxial tensile calculations were performed using classical MD modeling via the LAMMPS software package, which will also be used for subsequent fracture studies. A single sheet of GrE-2 with dimensions 21.5nm x 25.5nm (**Figure 2a**) held at 0 Kelvin was stretched by fixing one edge and displacing the opposing edge at a constant rate of 0.1 nm/ps for a strain rate of $0.5\cdot ns^{-1}$ which is of the same order as strain rates for other graphene fracture simulation studies[20, 21]. To achieve uniaxial stress, the boundaries normal to the direction of stretching are periodic, but permitted to relax (Figure 2a).

In-plane elastic modulii, and stress and strain to failure determined by DFT are reported in Table 1 for both directions of crystalline symmetry. Figure 2b shows the comparison between DFT and MD for tensile simulations. The results show that graphylene-2 is anisotropic, with the 1NN and 2NN directions having linear elastic modulii values of E_{2D} = 78.9 N/m and E_{2D} = 97.6 N/m respectively. The linear elastic modulus values are over three times smaller than that of pristine graphene, which is reported to be 340 N/m by numerous theoretical and experimental studies[11], but is still over 2× and 5× higher, per mass, than high performance engineering materials such as Kevlar and titanium, respectively[11] (based on an initial GrE-2 areal density of 6.53×10^{-7} kg/m^2). GrE-2 has a larger regime of nonlinear elastic response when compared to graphene, with the second-order term becoming more significant at lower strains.

The anisotropy of the mechanical properties in GrE-2 can be related to its structure. Virial stress mappings (see Supplemental Information) show that, at small strains, loads in the 1NN direction are primarily carried by the one ethylene chain per C_6 ring oriented in the 1NN direction, while the other ethylene chains are rotated without carrying significant tension. In contrast, loads in the 2NN direction are equally carried by two angled ethylene chains per C_6 ring, with the 1NN-oriented ethylene chains carrying a slight compression. This geometry suggests that the in-plane stiffness in the 2NN direction should be a factor of 1.5 times larger than the in-plane stiffness in the 1NN direction in the small strain limit, assuming perfectly stiff six-carbon rings (see Supplemental Information). This value is in reasonable agreement with the ratio of fitted linear elastic constants in the 2NN and 1NN directions, 1.24.

The predictions of elastic response of GrE-2 from the DFT and MD simulations are in good agreement (Figure 2a), indicating that the REBO potential is suitable for modeling graphylene polymers. However, the ultimate stress to failure of GrE-2 predicted by MD is significantly lower than that predicted by DFT. We attribute this discrepancy to the two possible causes. First, it may be that the 96-atom cell in the DFT simulation is insufficiently large to capture all failure modes in GrE-2. Secondly, the interaction cutoff imposed on the REBO potential[13, 15, 22] to prevent aphysical carbon-carbon scissioning that is a result of computational artifacts in the potential's switching function[23] may cause the discrepancy. While the MD simulations of GrE-2 may fail prematurely they will not contain any of the strain-hardening and high breaking strengths typical to REBO simulations without cutoffs. Therefore, the following MD simulations characterizing fracture behavior can be considered conservative, and that true intrinsic toughness values of graphylene may be even higher than our predictions.

Initiation of Mode-I Crack Growth in GrE-2 Graphylene

The mechanical properties of a pristine material are informative, but the practical load carrying ability of a structure is mitigated by imperfections and, more specifically, the comprising material's ability to tolerate such flaws while carrying stress. The intrinsic ability of a material to resist the initiation of crack growth from a pre-existing crack is referred to as fracture toughness. There are three metrics we use to quantify the fracture behavior of graphylene: i) *critical fracture energy* (quasi-static), G_{IC}, ii) *flaw-tolerance* (quasi-static) and iii) *fracture energy release rate* (dynamic), G_{2D}.

To characterize the critical fracture energy of graphylene, we performed MD simulations of fracture of a domain of GrE-2 with a pre-existing crack and compared the behavior to graphene under the same conditions. The crack domain, depicted in **Figure 3a**, is 60nm by 30nm which corresponds to an aspect ratio acceptable for modeling crack growth[24, 25] and matches the dimensions of previous MD simulations of graphene fracture[13]. The domain was permitted to relax in the direction perpendicular to strain and is non-periodic.

A pre-crack of length a_0 was created in the GrE-2 and graphene domains and strain was applied at a constant rate in the direction perpendicular to the pre-crack. This configuration is consistent with a mode-I crack, the results of which can be seen in Figure 3b. The crack width was 0.3nm and the crack tip radii were 0.15nm for consistency. To quantify fracture toughness we adopt a 2D formulation of the quasi-static critical fracture energy of a Griffith crack which is formulated assuming linear elasticity appropriate for the small (less than 5%) strain in our crack models:

$$G_{Ic,2D} = \frac{K_{Ic,2D}^2}{E_{2D}} = \frac{\sigma_{c,2D}^2}{2E_{2D}}\pi a_0 \qquad (2)$$

where $G_{Ic,2D}$ is the 2D mode-I critical fracture energy, $K_{Ic,2D}$ is the critical 2D mode-I stress concentration factor and $\sigma_{c,2D}$ is the 2D critical fracture stress. The critical fracture energy was first determined for graphene with a pre-crack length of a_0 of 10nm, resulting in a value of $G_{Ic,2D}$ = 2.28 nJ/m, in agreement with the critical fracture energy of graphene reported by a previous study, $G_{Ic,2D}$ = 2.33 nJ/m.[13] This value was found to be constant across all pre-crack lengths for the same domain dimensions, a signature of brittle material response. Examining the stress response of pre-cracked domains of graphene and GrE-2 (Figure 3b), it is evident that there are conditions where GrE-2 exhibits ductile fracture. At 300K and low strain rate, as well as 0K and high strain rate, GrE-2 exhibits ductile, stable crack growth. In contrast, graphene exhibits brittle failure for all cases.

A parametric study of pre-crack length was then performed for GrE-2, and the critical fracture energy can be seen in **Figure 3c** compared to that of graphene. Immediately it is clear that GrE-2, unlike graphene, has a critical fracture energy that is dependent on pre-crack length. Furthermore, the critical fracture energy of GrE-2, ($G_{Ic,2D}$ = 2.51 nJ/m at a_0 = 20 nm) exceeds that of graphene ($G_{Ic,2D}$ = 2.28 nJ/m across all pre-crack lengths) as pre-crack length increases. While GrE-2 shows initial crack growth at a lower critical stress than graphene, this initiation event occurs at a significantly higher strain than graphene.

Another fracture toughness metric, which we refer to as flaw tolerance, is the ratio of the strain energy of the flawed material relative to the strain energy of the pristine material[26]. The simulation results show that GrE-2 exhibits three times the value of this metric compared to graphene (**Figure 3d**). In other words, pre-existing defects in graphene will deteriorate the toughness of the material much more significantly than identical pre-existing defects in graphylene.

Crack initiation was also examined for a pre-crack oriented in the 1NN direction to compare to a pre-crack oriented in the 2NN direction at 0K and 300K (**Figure 4a**). It is evident that a mode-I crack oriented in the 1NN direction initiates growth at a significantly lower strain compared to a mode-I crack oriented along the 2NN direction, despite having similar global stress values at initiation. The critical fracture energies for the 1NN and 2NN GrE-2 mode-I directions at 0K are 1.78 nJ/m and 2.18 nJ/m, respectively. The difference in fracture toughness values in the two principal directions suggests that there are preferential crack propagation directions in GrE-2. This directionality is visually confirmed by examining the cracks after propagation, where the crack propagating along the 1NN direction (**Figure 4b**) has a straighter path than the 2NN direction (**Figure 4c**). Cracks preferentially propagate along the 1NN direction because, in this direction, straight pathways exist that avoid the high-strength C_6 rings. In other words, the weaker sp^3 bonds are broken while the stronger sp^2 bonds are left intact, similar to prior observations for crack initiation in randomly hydrogenized graphene[16] and crack propagation through sp^1 bond chains in graphynes[18]. In the 2NN direction, there is no direction in which the crack can advance without eventually encountering the C_6 rings. As such, we see more crack meandering when the flaw is oriented in the 2NN direction than when the flaw is oriented in the 1NN direction. The preferential crack propagation is also seen at 300K, albeit with a slightly lower critical fracture stress, and with additional ductile-like (non-critical) fracture behavior being exhibited. The implications of these meandering crack paths for energy absorption in graphylene are discussed in the following section.

Another contributing factor to enhanced fracture resistance in GrE-2 is crack tip bond topology. In a prior study[27], crack propagation in graphene was shown to be determined in part by the details of load sharing and bond rotations at the crack tip. Similarly, comparative calculations for GrE-2 and graphene with "sharp" crack tips (Supplemental Figure 4) show that cracks in GrE-2 converge to larger tip radii compared to crack tips in graphene, due to the larger lattice constant for GrE-2. The intrinsically blunter crack in GrE-2 results in a lower stress concentration factor, thereby increasing resistance to crack propagation. Furthermore, in graphene, cracks can propagate parallel to the zigzag direction without any bond rotations[27], while for GrE-2 there exist no directions for which fracture can propagate without some rotation of ethylene chains. These rotations contribute to the toughness of GrE-2 relative to graphene.

Crack Propagation in GrE-2 Graphylene

Although the critical fracture energy for graphene and graphylene are similar, this comparison only indicates the resistance of a material to initiation of crack growth from a pre-existing flaw. Also of significance is the manner in which the crack propagates. For graphene, our simulations confirm prior work indicating that graphene exhibits brittle crack propagation. In contrast, graphylene demonstrates behaviors characteristic of ductile material response. Fracture in GrE-2 was simulated at strain rates of 0.167ns^{-1} and 2.0ns^{-1} at 0K and 300K (**Figure 3b and Figure 4a**), all with the same domain and crack geometries. At higher strain rates and temperatures, GrE-2 exhibits stable crack propagation, as evidenced by the trailing decline of stress during crack propagation. In contrast, crack growth in graphene is unstable regardless of strain rate and temperature, and graphene is therefore consistently brittle.

To quantify the fracture energy release rate (the third metric we examine) as a crack propagates in a nonlinear elastic material[28], the instantaneous 2D energy release rate can be expressed at each strain increment as:

$$G_{2D} = -\frac{\partial(\Pi - W)}{\partial a} = -\frac{\partial \Pi}{\partial a}\bigg|_{\text{strain=const.}} \quad (3)$$

where G_{2D} is the energy release rate, $\prod$ is the potential energy of the system, W is external work and a is crack length. We ran simulations of crack propagation by creating a pre-crack of length a_0 = 10nm in a 60nm x 30nm domain at 0K, then imposing an initial condition of 5% strain on the domain by displacing the atoms along a linear gradient before time integration. Since strains are applied instantaneously and the displaced boundaries are held fixed while the crack propagates, then according to Equation (3) the energy release rate simply becomes the derivative of the system potential energy with respect to crack length.

The potential energy of this system is easily calculated, but the crack length is more difficult to quantify. To determine crack length, we plotted the atomic virial stress energy, Σ_{yy}, in the direction of strain and measured the distance between the stress concentrations on either crack tip, as seen in Figure 5a. This method also yielded average crack tip velocities, which are 14.9 km/s and 7.6 km/s for graphene and GrE-2 respectively. The system potential energy as a function of crack length for GrE-2 and graphene can be seen in Figure 5b. Under the same conditions, GrE-2 dissipates twice the energy (G_{2D} = 12.7 nJ/m) as graphene (G_{2D} = 6.5 nJ/m) during crack propagation. In other words, a crack in GrE-2 will grow half the length of a crack in graphene while dissipating the same amount of strain energy during propagation. In this regard, graphylene may be much tougher than graphene during dynamic crack propagation.

During fracture, two new surfaces within the material are created on either side of the crack. Griffith theory suggests that in an ideal case the fracture energy for a material should therefore have a lower bound of $G = 2\gamma$, where γ is surface energy. In reality, for crystalline materials there are factors that make the fracture energy larger than this theoretical lower limit. Lattice trapping, which is the added resistance of overcoming a periodic energy barrier such as a crack propagating through a crystal lattice, has been experimentally and theoretically demonstrated to increase critical fracture energy beyond the Griffith lower limit[29-31]. A combined ab-initio and molecular dynamics study has shown lattice trapping to be significant in graphene sheets during fracture, causing the G to have a value 10-20% larger than 2γ[32]. We calculated the surface energy of graphene (described in the Supplemental) to have a value of 2γ = 5.9 nJ/m and GrE-2 to have a value of 2γ = 9.8 nJ/m. Normalizing our G_{2D} values by these surface energy values, we see that the ratio of $G/2\gamma$ is 1.1 for graphene, in agreement with the prior study[32], and 1.3 for GrE-2, suggesting that lattice trapping could be an important contributor to ductile fracture behavior in GrE-2.

During crack growth under constant strain, GrE-2 begins to exhibit fracture characteristics of a ductile material (**Figure 4e**). GrE-2 crack morphologies consistent with ductile fracture include i) bridging, ii) meandering, and iii) plastic deformation ahead of the crack tip. Moreover, the formation of daughter cracks is evident. The minor meandering of the crack, also known as hackling, in GrE-2 can be attributed to several factors. Foremost, as shown in Fig. 4, the inherent anisotropy of the polymer structure leads to preferential crack directions, meaning that a mode-I crack may deviate from propagating perpendicular to the direction of strain in order to pursue preferential crystalline directions. Secondly, nonlinear elastic materials have been shown to experience hackling. In the high strain regions around the crack tip in a nonlinear elastic material, the material will soften in varying directions, causing the crack to propagate at random angles to pursue the path of least resistance[24].

All of these fracture characteristics are energy dissipation mechanisms, allowing for GrE-2 to resist the advancement of cracks more readily than graphene. In comparison, graphene has a perfectly mirrored fracture pattern (**Figure 4f**), characteristic of brittle facture, with no features to assist in dissipating energy. Graphylene also reveals its ductile nature during the constant strain rate fracture simulations at 300 K and at 0 K with a strain rate of 2ns^{-1} (Figure 3b). When the critical stress has been reached under these conditions, the crack propagates, but still maintains a decreasing stress until the crack finishes propagating across the domain.

Conclusions

The simulations in this study suggest that GrE-2 graphylene exhibits features consistent with ductile fracture propagation, in contrast to the brittle fracture that has been predicted and observed for graphene. Furthermore, GrE-2's compliant structure gives it i) three times as flaw-tolerance of graphene, ii) twice the fracture energy release rate during propagation as graphene, and iii) greater quasi-static critical fracture energy as graphene in the cases we examined. Combined with its very high stiffness and strength relative to current engineering materials, graphylene possesses a unique set of mechanical properties that could enable engineering structures with unprecedented performance. Although not presented here, simulations of the transport and electronic properties of graphylene are also underway.

The present GrE-2 graphylene polymer is a useful model system, in particular considering the maturity of DFT and MD bond potential functions for the comprising benzene and polyethylene subcomponents of the structure. However, a nearly limitless range of 2D polymers can be imagined, providing ample opportunity for further study and improvement in properties. The practical realization of these materials will require parallel mechanical modeling and synthesis efforts to identify systems with useful properties that can also be readily fabricated.

While we have observed ductile-like fracture mechanisms in monolayer GrE-2, the calculated fracture toughness for a single atomic sheet of graphylene is orders of magnitude lower than established values for macroscale ductile materials such as metals, alloys and bulk polymers. However, the comparison of monolayer fracture with bulk fracture behavior is short-sighted, since macroscopic mechanical properties such as toughness and ductility emerge from physical features that range across multiple length scales. Additionally, ductility and plasticity are inherently three-dimensional phenomena that are a result of developments such as propagation of dislocations, inter-granular sliding, internal friction between polymer crystallites, and are not present in the consideration of a single 2D monolayer. Therefore, the present results indicate how a 2D bond network can be tailored to reduce brittle fracture propagation, but bulk ductility requires the study of many interacting layers of material. In fact, bulk 2D polymer systems for engineering applications will require hundreds, thousands, or millions of layers, and may take the form of ensembles of finite-sized molecules rather than effectively infinite sheets. The interactions between these layers or molecules will to great extent determine the bulk behavior of these systems. Simulation and design of these interfaces will be crucial for realization of the potential for these materials.

Simulation Methodology

Density Functional Theory. We used the CP2K software package for our structural and elasticity calculations. This code employs the Quick-Step method outlined by VendeVondele *et al.*[33], and we implement the generalized gradient approximation exchange-correlation functional BLYP due to Becke[34] and Lee, Yang, Parr[35]. For the uniaxial stress curves a script was used to relax the lateral stresses in an iterative fashion. Starting from the fully relaxed zero stress structure (within 100 bar) a uniaxial strain of 0.01 was applied. The system was then allowed to relax using geometry optimization. If the lateral stress was found to be non-zero (within tolerance) the lateral dimension was adjusted so as to relieve the stress. Geometry optimization was again performed and the process repeated until the lateral stress was reduced to zero (again within tolerance) so that the strain is finally uniaxial. At this point an additional uniaxial strain of 0.01 with respect to the relaxed structure is applied and the process repeated for the new strain. The whole process is continued until the structure fails (within the theory) and a uniaxial stress-strain curve is generated.

Molecular Dynamics. Classical molecular dynamics simulations are performed using the LAMMPS software package. Because of its well-documented accuracy in predicting the mechanical behavior of hydrocarbon systems (including fracture), the REBO potential [36] was used with a cutoff of 0.197nm, consistent with other literature involving carbon-carbon scissioning [13, 15, 22] and a time step of 1fs. The unit cell and basis vector for the GrE-2 polymer as determined by DFT were also used as an initial condition for classical MD simulation. All simulations were performed by bringing the ensemble to the desired initial temperature using a Berendsen thermostat, and then releasing the thermostat and time integrating at constant energy (NVE).

Acknowledgements

This research was supported in part by an appointment to the Postgraduate Research Participation Program at the U.S. Army Research Laboratory administered by the Oak Ridge Institute for Science and Education through an interagency agreement between the U.S. Department of Energy and USARL.

Notes and references

1. Kory, M. J.; Wörle, M.; Weber, T.; Payamyar, P.; van de Poll, S. W.; Dshemuchadse, J.; Trapp, N.; Schlüter, A. D. *Nature chemistry* **2014,** 6, (9), 779-784.
2. Gupta, A.; Sakthivel, T.; Seal, S. *Progress in Materials Science* **2015,** 73, (0), 44-126.
3. Treier, M.; Pignedoli, C. A.; Laino, T.; Rieger, R.; Müllen, K.; Passerone, D.; Fasel, R. *Nature chemistry* **2011,** 3, (1), 61-67.
4. Kissel, P.; Erni, R.; Schweizer, W. B.; Rossell, M. D.; King, B. T.; Bauer, T.; Götzinger, S.; Schlüter, A. D.; Sakamoto, J. *Nature chemistry* **2012,** 4, (4), 287-291.
5. Payamyar, P.; Kaja, K.; Ruiz-Vargas, C.; Stemmer, A.; Murray, D. J.; Johnson, C. J.; King, B. T.; Schiffmann, F.; VandeVondele, J.; Renn, A. *Advanced Materials* **2014,** 26, (13), 2052-2058.
6. Xu, H.; Gao, J.; Jiang, D. *Nature Chemistry* **2015,** 7, (11), 905-912.
7. Lee, C.; Wei, X.; Kysar, J. W.; Hone, J. *Science* **2008,** 321, (5887), 385-8.
8. Petrone, N.; Dean, C. R.; Meric, I.; Van Der Zande, A. M.; Huang, P. Y.; Wang, L.; Muller, D.; Shepard, K. L.; Hone, J. *Nano Letters* **2012,** 12, (6), 2751-2756.
9. Lee, G.-H.; Cooper, R. C.; An, S. J.; Lee, S.; van der Zande, A.; Petrone, N.; Hammerberg, A. G.; Lee, C.; Crawford, B.; Oliver, W.; Kysar, J. W.; Hone, J. *science* **2013,** 340, (6136), 1073-1076.
10. Grantab, R.; Shenoy, V. B.; Ruoff, R. S. *Science* **2010,** 330, (Copyright 2010, The Institution of Engineering and Technology), 946-8.
11. Wetzel, E. D.; Balu, R.; Beaudet, T. D. *Journal of the Mechanics and Physics of Solids* **2015,** 82, (0), 23-31.
12. Lee, J.-H.; Loya, P. E.; Lou, J.; Thomas, E. L. *science* **2014,** 346, (6213), 1092-1096.
13. Zhang, P.; Ma, L.; Fan, F.; Zeng, Z.; Peng, C.; Loya, P. E.; Liu, Z.; Gong, Y.; Zhang, J.; Zhang, X. *Nature communications* **2014,** 5.
14. Hwangbo, Y.; Lee, C.-K.; Kim, S.-M.; Kim, J.-H.; Kim, K.-S.; Jang, B.; Lee, H.-J.; Lee, S.-K.; Kim, S.-S.; Ahn, J.-H. *Scientific reports* **2014,** 4.
15. Pei, Q.; Zhang, Y.; Shenoy, V. *Carbon* **2010,** 48, (3), 898-904.
16. Li, Y.; Datta, D.; Li, Z.; Shenoy, V. B. *Computational Materials Science* **2014,** 83, 212-216.
17. Cranford, S. W.; Buehler, M. J. *Carbon* **2011,** 49, (13), 4111-4121.
18. Cranford, S. W.; Brommer, D. B.; Buehler, M. J. *Nanoscale* **2012,** 4, (24), 7797-7809.
19. Brommer, D. B.; Buehler, M. J. *Journal of Applied Mechanics* **2013,** 80, (4), 040908-040908.
20. Zhang, Z.; Wang, X.; Lee, J. D. *Journal of Applied Physics* **2014,** 115, (11), -.
21. Le, M.-Q.; Batra, R. C. *Computational Materials Science* **2013,** 69, (0), 381-388.
22. Grantab, R.; Shenoy, V. B.; Ruoff, R. S. *science* **2010,** 330, (6006), 946-948.
23. Pastewka, L.; Pou, P.; Pérez, R.; Gumbsch, P.; Moseler, M. *Physical Review B* **2008,** 78, (16), 161402.

24. Buehler, M. J.; Gao, H. *Dynamic* **2006**, 1.
25. Cleri, F.; Phillpot, S. R.; Wolf, D.; Yip, S. *J. Am. Ceram. Soc.* **1998,** 81, (3), 501-516.
26. Markus, J. B.; Haimin, Y.; Huajian, G.; Baohua, J. *Modelling and Simulation in Materials Science and Engineering* **2006,** 14, (5), 799.
27. Datta, D.; Nadimpalli, S. P. V.; Li, Y.; Shenoy, V. B. *Extreme Mechanics Letters* **2015,** 5, 10-17.
28. Aït-Bachir, M.; Mars, W. V.; Verron, E. *International Journal of Non-Linear Mechanics* **2012,** 47, (4), 22-29.
29. Thomson, R.; Hsieh, C.; Rana, V. *Journal of Applied Physics* **1971,** 42, (8), 3154-3160.
30. Curtin, W. *Journal of Materials Research* **1990,** 5, (07), 1549-1560.
31. Bernstein, N.; Hess, D. W. *Physical Review Letters* **2003,** 91, (2), 025501.
32. Khare, R.; Mielke, S. L.; Paci, J. T.; Zhang, S.; Ballarini, R.; Schatz, G. C.; Belytschko, T. *Physical Review B* **2007,** 75, (7), 075412.
33. VandeVondele, J.; Krack, M.; Mohamed, F.; Parrinello, M.; Chassaing, T.; Hutter, J. *Computer Physics Communications* **2005,** 167, (2), 103-128.
34. Becke, A. D. *Physical review A* **1988,** 38, (6), 3098.
35. Lee, C.; Yang, W.; Parr, R. G. *Physical review B* **1988,** 37, (2), 785.
36. Stuart, S. J.; Tutein, A. B.; Harrison, J. A. *The Journal of chemical physics* **2000,** 112, (14), 6472-6486.

Figure Legends

Figure 1: Graphylene-2 in a) "System A" b) "System B" configurations with grey and red indicating carbon and hydrogen atoms respectively. System B has carbon atoms above and below the center plane of the material. c) Enthalpy of System A / System B GrE-2 with unit cells inlaid. First and second nearest neighbor directions of System B are denoted by the axes marked 1NN and 2NN respectively.

Figure 2: a) MD domain and boundary conditions for modeling GrE-2 under uniaxial tension. Hydrogen atoms are not depicted for ease of viewing. b) Predicted 1st Piola-Kirchhoff stress vs. engineering strain for uniaxial tension simulations of GrE-2 to failure using both DFT and MD in 1NN and 2NN directions. Inlays depict deformed lattices (from MD simulations) in both directions at 12.5% strain. Solid lines depict curve fits of Eq. 1 to the DFT data.

Figure 3: a) Crack domain of GrE-2 to examine fracture toughness, b) nominal stress vs. nominal strain of graphene and a GrE-2 Griffith crack propagating along the 2NN direction at various conditions (a_0=10nm), c) the critical fracture energy of graphene and GrE-2 at varying initial crack lengths initialized at 0 K, and d) comparison in stress-strain response between pristine and cracked graphene and GrE-2 at 0K demonstrating superior flaw tolerance of GrE-2.

Figure 4: a) nominal stress vs. nominal strain for the same the same initial length (a_0=10nm) of a crack propagating through the 1NN and 2NN GrE-2 directions initialized at 0K and 300K. b) Straight 1NN-oriented crack in GrE-2 while being strained in the perpendicular direction, strain rate of 0.167 ns^{-1}, at 0 K and c) Meandering (hackling) crack oriented along the 2NN direction in GrE-2 while being strained in the perpendicular direction, strain rate of 0.167 ns^{-1} at 0 K.

Figure 5: a) Crack length, *a*, as defined by the concentration of virial stress energy of the carbon atoms of GrE-2 during crack propagation at 0K and a strain rate of 0.167ns^{-1}, stretched in the 1NN direction and b) system potential during crack growth with fixed strain displacement in the 1NN direction for graphene and GrE-2. The domain is displaced perpendicular to the crack, at an initial instantaneous strain of 5% and initialized at temperature of 0 K. c) A crack in GrE-2 during propagation at an initial instantaneous strain of 5%, 0K with features of ductile fracture including daughter cracks, hackling, and bridging. d) A mirror crack in graphene during propagation at constant strain of 5%, 0K. All pre-crack lengths are a_0=10nm.

Tables

Table 1: In-mechanical properties of GrE-2 determined from DFT. First and second nearest neighbor directions are denoted as 1NN and 2NN respectively.

	E_{2D} [N/m]	D_{2D} [N/m]	σ_f [N/m]	ϵ_f [-]
1NN	78.9	-84.7	11.4	0.19
2NN	97.6	-245.0	16.4	0.23